

Utah State University

DigitalCommons@USU

Electrical and Computer Engineering Student
Research

Electrical and Computer Engineering Student
Works

1-21-2020

Design of Hypervelocity-Impact Damage Evaluation Technique Based on Bayesian Classifier of Transient Temperature Attributes

Haonan Zhang

University of Electronic Science and Technology of China

Xuegang Huang

China Aerodynamics Research and Development Center

Chun Yin

University of Electronic Science and Technology of China, yinchun.86416@163.com

Yu-Hua Cheng

University of Electronic Science and Technology of China

Anhua Shi

China Aerodynamics Research and Development Center

Sara Dadras

Utah State University, s_dadras@ieee.org

Follow this and additional works at: https://digitalcommons.usu.edu/ece_stures
See next page for additional authors

Recommended Citation

H. Zhang et al., "Design of Hypervelocity-Impact Damage Evaluation Technique Based on Bayesian Classifier of Transient Temperature Attributes," in *IEEE Access*, vol. 8, pp. 18703-18715, 2020.
<https://doi.org/10.1109/ACCESS.2020.2968398>

This Article is brought to you for free and open access by the Electrical and Computer Engineering Student Works at DigitalCommons@USU. It has been accepted for inclusion in Electrical and Computer Engineering Student Research by an authorized administrator of DigitalCommons@USU. For more information, please contact digitalcommons@usu.edu.



Authors

Haonan Zhang, Xuegang Huang, Chun Yin, Yu-Hua Cheng, Anhua Shi, Sara Dadras, and Jinyang Luo

Received November 21, 2019, accepted December 26, 2019, date of publication January 21, 2020, date of current version January 30, 2020.

Digital Object Identifier 10.1109/ACCESS.2020.2968398

Design of Hypervelocity-Impact Damage Evaluation Technique Based on Bayesian Classifier of Transient Temperature Attributes

HAONAN ZHANG^{1,*}, XUEGANG HUANG^{2,*}, CHUN YIN¹, (Member, IEEE),
YU-HUA CHENG¹, ANHUA SHI², SARA DADRAS³, (Senior Member, IEEE),
AND JINYANG LUO²

¹School of Automation Engineering, University of Electronic Science and Technology of China, Chengdu 611731, China

²Hypervelocity Aerodynamics Institute, China Aerodynamics Research and Development Center, Mianyang 621000, China

³Electrical and Computer Engineering Department, Utah State University, Logan, UT 84321, USA

Corresponding author: Chun Yin (yinchun.86416@163.com)

This work was supported in part by the National Basic Research Program of China under Grant 61873305 and Grant U1830207, and in part by the Sichuan Science and Technology Plan Project under Grant 2019YJ0199 and Grant 2018JY0410.

*Haonan Zhang and Xuegang Huang contributed equally to this work.

ABSTRACT With the rapid increasement of space debris on earth orbit, the hypervelocity-impact (HVI) of space debris can cause some serious damages to the spacecraft, which can affect the operation security and reliability of spacecraft. Therefore, the damage detection of the spacecrafts has become an urgent problem to be solved. In this paper, a method is proposed to detect the damage of spacecraft. Firstly, a variable-interval method is proposed to extract the effective information from the infrared image sequence. Secondly, in order to mine the physical meaning of the thermal image sequence, five attributes are used to construct a feature space. After that, a Naive Bayesian classifier is established to mine the information of different damaged areas. Then, a maximum interclass distance function is used choose the representative of each class. Finally, in order to visualize damaged areas, the Canny operator is used to extract the edge of the damage. In the experiment, ground tests are used to simulate hypervelocity impacts in space. Historical data of natural damaged material and artificial damaged material are used to build different classifiers. After that, the effective of classifiers is illustrated by accuracy, F-score and AUC. Then, two different types of materials are detected by proposed method, Independent Component Analysis (ICA) and Fuzzy C-means (FCM). The results show that the proposed method is more accurate than other methods.

INDEX TERMS Damage evaluation, transient temperature attributes, hypervelocity impact, Bayesian classifier.

I. INTRODUCTION

In recent years, more and more rockets, satellites and probes are launched into the earth's orbit [1], [2]. Collisions or explosions of these objects have caused a great deal of fragments in all kinds of sizes and shapes and over the years [3], [4]. In recent years, the HVI risk from meteoroid/orbital debris (M/OD) has become one of the main threats to space activities [5], [6], as displayed in Figures 1-2. Due to the randomness of M/OD impact events, the impact parameters

The associate editor coordinating the review of this manuscript and approving it for publication was Xin Luo.

are unpredictable [7]–[9]. To guarantee that M/OD risk assessments are applied for spacecrafts, some effective nondestructive testing technologies should be evaluated for the M/OD impact damages.

Infrared thermography method would be an effective method for damage detection, since that it is a widely applied NDT method with short detection time and does not require direct contact with the specimen [12], [13]. In the process of detection, the distribution of the Joule heat can be affected by the location of the damages. It is common that the high Joule heat leads to high temperature areas and the low Joule heat leads to low temperature areas [14]. After that, infrared

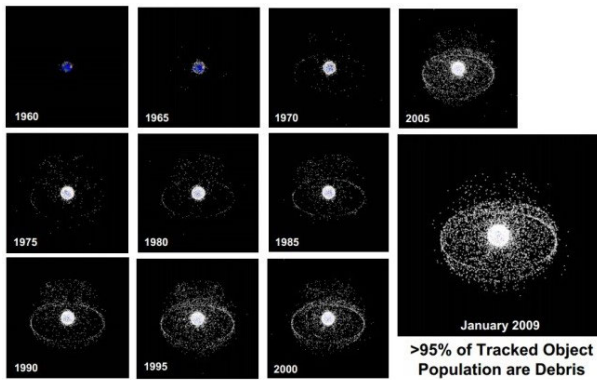


FIGURE 1. Development of space debris environment in [5].

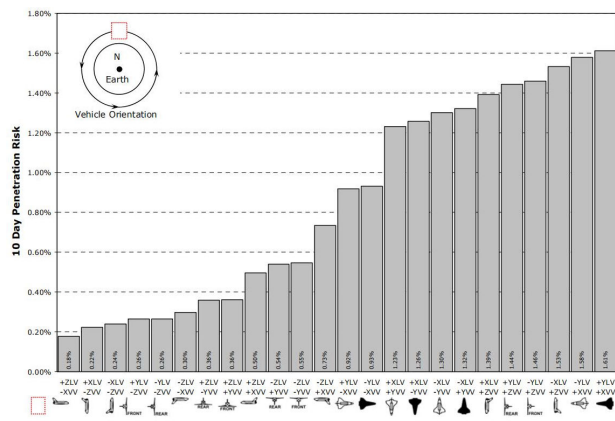


FIGURE 2. The probability of spacecraft failure in [5].

camera is used to record the thermal image sequence of specimen and the damage information can be obtained by image sequence.

Recently, there are many algorithms in extracting the damage feature of thermal image sequence, such as independent components analysis (ICA) [15], [16], principal components analysis (PCA) [17], [19]. Both of them focus on the processing of the thermal image sequence. Specifically, ICA in [18] is mainly used to extract the information of surface defects. PCA is applied in [19] to extract the different damage types. Recently, the other researches [20]–[22] studied how to exact the damage information by classifying temperature points of different regions in the image sequence. To search the representative temperature points, the works [20]–[22] adopted K-means and FCM algorithm to distinguish the temperature changes in different positions. These methods in [20]–[22] do not apply target attributes, rather they classify the dataset by using similarity measures [30]. In addition, these methods are not suitable for noisy high-dimensional data [31] and it is hard to know which clustering model is correct and which is the best [32]. Actually, it can be found that the temperature variation of each pixel in the image sequence can be described by some physical attributes, such as temperature change rate, energy, etc. The data set of attributes distribution can be established by mining the physical attributes of historical data. It could be used to build the probabilistic-expression

of any physical attribute to be divided in different damage regions. In order to reduce the influence of noise on the division of TTRs and to divide the TTRs by physical attributes, the Bayesian theory is investigated. Naive Bayesian classifier (NB), which assumes that each attribute is conditional independence and has the same impact on the classification, is an effective way to extract the main information. The Bayesian classifier as a data classification method has been developed to calculate probability of category differentiation in a series of practical problems [23]–[25]. For example, Da Silva *et al.* [25] use NB for detection of transmission line damage. In [24], it is used for detecting the welded joints based on vibration signals. Thus, it should be a good solution that developing a NB classifier for HVI damage detection, while considering how to classify temperature points of different regions more accurately.

This paper proposes transient temperature attributes to describe the thermal image sequence of the HVI damage evaluation. Moreover, the five transient temperature attributes are applied to build the feature space of the impact evaluation. With the help of the feature space, a variable-interval method is established to seek TTRs from the thermal image sequence. A Bayesian classifier of transient temperature attributes is further built to classify the searched TTRs, to distinguish the temperature changes in different positions. Moreover, the most effective TTRs of different regions can be determined by a maximum-interclass distance function, to make the damage evaluation more efficient. To make the result visible, the Canny operator [26], [27] is used to extract the edge of the images. In the experiment, two types of aerospace materials with impact damage and artificial damage are utilized to verify the effectiveness and accuracy of the developed method. The main works of this paper are listed as follows: 1) A detection framework for HVI damage assessment is proposed. 2) Some physical features to fully exploit the features to TTR are proposed. 3) A Bayesian classifier is built through the features of TTR, which improves the accuracy of traditional methods.

II. DETECTION FRAMEWORK

Space debris with different size cause varying degrees of impact damage on spacecraft [5]: the ground-based radars or optical-sensor systems can follow the trail of the large-size M/OD objects from *m* to *cm* scales, to avoid the impact events of spacecraft. However, the small-size M/OD in *mm* and μ scales cannot be monitored, so the hypervelocity impacts become inevitable and more dangerous because that the number of small-size M/OD is very high. Obviously, the damage evaluation is very important in the impact risk assessment of M/OD accordingly. Therefore, it should be valuable to evaluate the M/OD HVI damages with a few of effective non-destructive testing methods, which could be also necessary for the M/OD protection design and the ground HVI test for various spacecrafts.

The infrared thermal imaging technology is a fast, convenient and non-contact method that can be used to determine

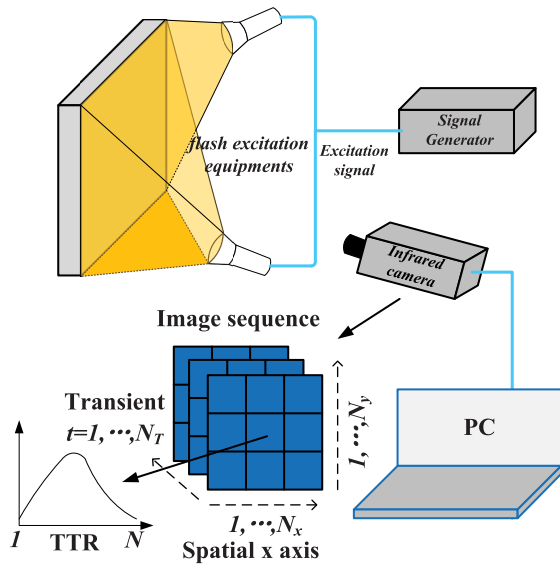


FIGURE 3. Infrared thermography defect detection system.

hypervelocity impact damage by recording heat distribution in different areas. In this study, a detection framework based on infrared technology, which does not cause secondary material damage, is proposed to detect the damage of spacecraft material. The infrared technology is considered to be a fast and efficient tool for spacecraft damage detection. It can effectively record the heat distribution of the material, and these collected data can be called the thermal image sequence. An infrared thermography defect detection system is shown in Figure 3. The signal generator is used to generate the excitation signal, which is a small period of high frequency current. It is applied to drive the flash excitation equipments on the material. Then, the flash excitation equipments will induce light energy and generate heat in the material. Finally, an infrared camera is used to collect the heat distribution of the material.

In general, the image sequence can be represented by a three-dimensional matrix block ($S \in R^{N_I \times N_J \times N_T}$), where $N_I \times N_J$ represents the size of each image and N_T represents the number of frames. In the image sequence, each pixel counts the temperature change of the corresponding location of the material. The temperature changes of each pixel is defined as the temperature transient response (TTR). The typical TTRs are shown in Figure 4. Since media in different damaged areas are different, the heat transfer process is different and this can cause the differences of TTRs in different damaged areas. Hence, different damaged areas can be identified by judging the difference of TTRs.

As shown in Figure 5, this detection framework mainly contains three steps. In order to remove redundant TTRs, a variable-interval method is proposed. In order to judge TTRs in different damaged areas, some attributes are proposed to mine the physical features of TTRs, and then a Bayesian classifier is built based on physical attributes. Finally, in order to realize damage visualization, a maximum interclass distance function is used to select representatives

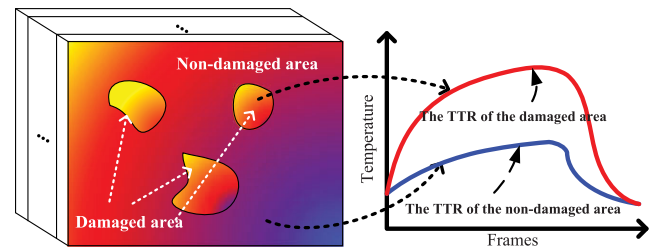


FIGURE 4. The differences of TTRs.

to reconstruct damage images and the Canny operator is used to measure the edge information. Finally, we can assess the damage of the material by these images.

III. PROPOSED METHOD

This section will introduce the proposed detection framework in the following.

A. VARIABLE-INTERVAL METHOD

In the collected infrared image sequences, there are many TTRs with little difference. Obviously, these redundant TTRs can affect the efficiency of the detection framework. As shown in Figure 6, blue and red area represents non-damaged and damaged area respectively. TTRs are taken from different areas (that is, TTR1 and TTR2 are taken from the non-damaged area, TTR3 and TTR4 are taken from the damaged region). They are further drawn in the coordinates. It can be found that TTRs in the same area are similar (TTR1 is similar as TTR2, TTR3 is similar as TTR4). Moreover, these similar redundant TTRs can cause repeated computation in the classifier. Hence, a variable-interval method is proposed to extract the effective information of the image sequence. The method comprises the following steps:

Step 1: Input $S \in R^{N_I \times N_J \times N_T}$ and define the temperature change rate (TCR) $V(i, j) = \frac{S(i, j, t_{mid}) - S(i, j, t_0)}{t_{mid} - t_0}$. The global TCR can be represented by $S(I^*, J^*, :)$, where $I^* = \arg \max_i V(i, j)$, $J^* = \arg \max_j V(i, j)$. Then, search the global maximum temperature $S(I^*, J^*, T^*)$ from $S(I^*, J^*, :)$, in which $T^* = \arg \max_t S(I^*, J^*, t)$.

Step 2: Set the temperature $T(q)$, $q = 1, \dots, Q$ to divide the column of $S(I^*, J^*, T^*)$ into $Q + 1$ data blocks. Then, calculate the TCR of the TTRs in the v^{th} block, i.e. $V^v(i, J^*) = \frac{S^v(i, J^*, t_{mid}) - S^v(i, J^*, t_0)}{t_{mid} - t_0}$, where $v = 1, \dots, Q + 1$. After that, the Pearson correlation coefficient Re_{RL}^v is calculated between $S^v(I^{v*}, J^*, :)$ and each TTR in the v^{th} block, where $I^{v*} = \arg \max_i (V^v(i, J^*))$. Start the search from both sides of $S^v(I^{v*}, J^*, :)$; if $Re_{RL}^v \geq Th_{RL}^v$, then $RL^v = RL^v + 1$, until $Re_{RL}^v < Th_{RL}^v$, where Th_{RL}^v represents the correlation threshold, and RL^v is the row interval, which is initialized to 0. Then, go to Step 3.

Step 3: Set the temperature $T(p)$, $p = 1, \dots, P$ to divide the row of $S(I^*, J^*, T^*)$ into $P + 1$ data blocks. Then, calculate the TCR of the TTRs in the u^{th} block, i.e. $V^u(I^*, j) = \frac{S^u(I^*, j, t_{mid}) - S^u(I^*, j, t_0)}{t_{mid} - t_0}$, where $u = 1, \dots, P + 1$. Next, compute

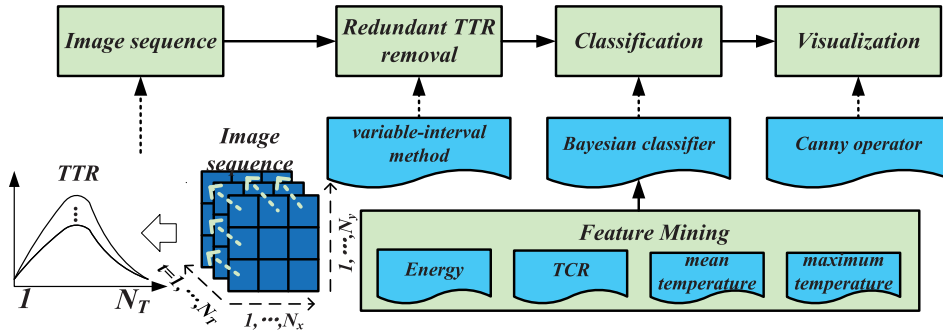


FIGURE 5. The detection framework.

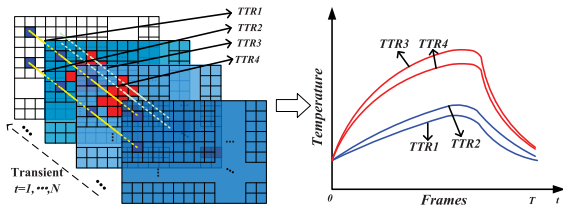


FIGURE 6. Redundant TTRs.

the PCC (Re_{CL}^u) between $S^u(I^*, J^{u*}, :)$ and each TTR in the u^{th} block, where $J^{u*} = \arg \max(V^u(I^*, j))$. Start the search from both sides of $S^u(I^*, J^{u*}, :)$; if $Re_{CL}^u \geq Th_{CL}^u$, then $CL^u = CL^u + 1$, until $Re_{CL}^u < Th_{CL}^u$, where Th_{CL}^u represents the correlation threshold, and CL^u is the row interval, which is initialized to 0. Then, go to Step 4.

Step 4: Initialize $k = 1$ and set $X(:, 1) = S(I^*, J^*, :)$. Then, compute the Pearson correlation coefficient Re between $X(:, k)$ and $S(i, j, :)$, where $i = 1 : n_v \cdot RL^v : 1 + n_{Q+1} \cdot RL^{Q+1}$ and $j = 1 : m_u \cdot CL^u : 1 + m_{P+1} \cdot CL^{P+1}$. n_v and m_u represent the maximum number of sampling points in the v^{th} block and the u^{th} block respectively. If $Re < Th$, then $k = k + 1$ and set $X(:, k) = S(i, j, :)$, otherwise remove $S(i, j, :)$.

Based on transient temperature attributes, the TTRs X can be further extracted from the TTRs of the image sequence by utilizing the proposed method. As shown in Figure 7, the temperature change rate (TCR, $V(i, j) = \frac{S(i, j, t_{mid}) - S(i, j, t_0)}{t_{mid} - t_0}$) is used to find the global maximum temperature ($S(I^*, J^*, T^*)$). Then, according to $S(I^*, J^*, T^*)$, $T(p)$ and $T(q)$, S is divided into small data block. After that, CL^u and RL^v are obtained by calculating TCR ($V^u(i, j)$ and $V^v(i, j)$) and correlation coefficient (Re_{CL}^u and Re_{RL}^v). Next, image sequence (S) is sampled through CL^u and RL^v , and then Re is calculated. Finally, the effective information is obtained.

B. BAYESIAN CLASSIFIER

After removing the redundant information, TTRs in different damaged areas should be distinguished. In this subsection, the prior information is used to establish a Bayesian classifier and the classifier is used to judge TTRs in different damaged areas.

1) FEATURE EXTRACTION

TTRs are different in different areas since thermal media are different in different types of damaged areas, and they can be described by some physical features through observation. Hence, some physical features are proposed in this subsection to extract the characteristics of the TTR, and these attributes are quantified as follows:

1. Energy (E)

$$E^i = \|X^i\|_2^2 = x_1^i{}^2 + x_2^i{}^2 + \dots + x_{N_T}^i{}^2, \tag{1}$$

where $X^i = (x_1^i, x_2^i, \dots, x_{N_T}^i)$ represents the i^{th} TTR.

2. TCR during endothermic process (V_{up})

$$V_{up}^i = \tan \alpha_i = \frac{x_{t_{mid}}^i - x_{t_0}^i}{t_{mid} - t_0}, \tag{2}$$

where the endothermic process is from t_0 to t_{mid} . α represents the angle between the horizontal direction and the line between $x_{t_0}^i$ and $x_{t_{mid}}^i$.

3. TCR during the exothermic process (V_{down})

$$V_{down}^i = \tan \beta_i = \frac{x_{t_{mid}}^i - x_{N_T}^i}{N_T - t_{mid}}, \tag{3}$$

where β represents the angle between the horizontal direction and the line between $x_{t_{mid}}^i$ and $x_{N_T}^i$.

4. Mean temperature (T_{ave})

$$T_{ave}^i = \frac{\sum_{t=1}^{N_T} x_t^i}{N_T}. \tag{4}$$

5. Maximum temperature (T_{max})

$$T_{max}^i = \max_{t=1, \dots, N_T} x_t^i. \tag{5}$$

The corresponding TTR of damaged area (red) and the corresponding TTR of non-damaged area (blue) are shown in Figure 8. E is described by the shaded areas. V_{up} and V_{down} are displayed by the black and blue dotted line. Purple and green dotted line are used to represent T_{max} and T_{ave} respectively. Since that these attributes are unequal between different areas, they can be used to build the feature space for damage identification.

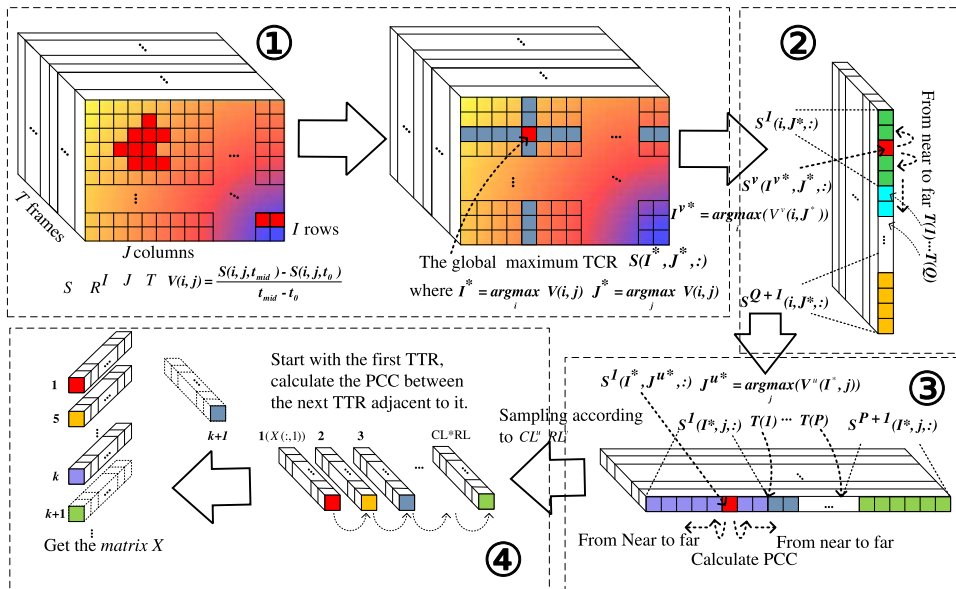


FIGURE 7. The frame of variable sampling method.

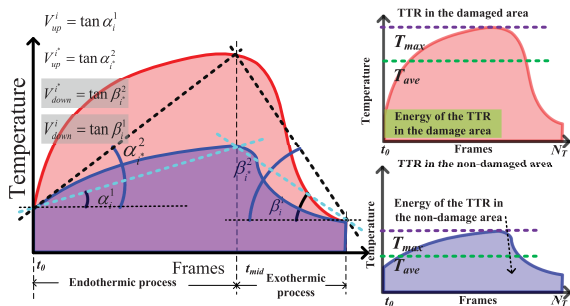


FIGURE 8. The features of TTRs.

The differences of represented TTPs exacted from TTRs can be used to identify the damaged areas. It is worth mentioning that previous methods distinguish TTRs of different areas by distance or correlation, for example, the correlation function was proposed in our previous works [20], [21] and FCM was applied in [22]. Although their results are reliable, they do not make full use of the prior information. In addition, since these methods directly process the TTR in the time domain, the classification factors are relatively simple. These issues may affect the accuracy of identifying damaged areas.

2) ESTABLISHMENT OF BAYESIAN CLASSIFIER

In order to improve the accuracy of damaged areas identification, Bayesian classifier is used to mine the difference of TTRs in different areas based on the historical data. The details are as follows:

As proposed in Section III, the transient temperature attributes can be used to describe TTPs. Therefore, the i -th TTP $X(:, i)$ can be labeled by $\bar{X}^i = (E^i, V_{up}^i, V_{down}^i, T_{ave}^i, T_{max}^i)$. In addition, $c_k, k = 1, 2, \dots, K$

TABLE 1. Description of feature discretization.

| | E^i | V_{up}^i | V_{down}^i | T_{ave}^i | T_{max}^i |
|---|--------|------------|--------------|-------------|-------------|
| 1 | high | fast | fast | high | high |
| 2 | higher | faster | faster | higher | higher |
| 3 | lower | slower | slower | lower | lower |
| 4 | low | slow | slow | low | low |

are used to represent the different damaged areas. Before the construction of the Bayesian classifier, the continuous feature values are discretized by the discretization-method given in [28], the results are shown in Table 1. From the Bayesian theorem, the posteriori probability is given by $p(c_k | \bar{X}^i) = \frac{p(\bar{X}^i | c_k) p(c_k)}{p(\bar{X}^i)}$, where $p(\bar{X}^i | c_k)$ denotes the likelihood that indicates the distribution of TTR \bar{X}^i in different areas. $p(c_k)$ represents the priori probability of class c_k .

Since the Bayesian classifier has the conditional independence assumption, the likelihood is further denoted as follows:

$$p(\bar{X}^i | c_k) = p(E^i | c_k) \cdot p(V_{up}^i | c_k) \cdot p(V_{down}^i | c_k) \cdot p(T_{ave}^i | c_k) \cdot p(T_{max}^i | c_k) \quad (6)$$

In Bayesian classifier, the category with the greatest posterior probability is considered as the category of the TTR \bar{X}^i , i.e. $h_{nb}(\bar{X}^i) = \arg \max_{c_k \in C} p(c_k | \bar{X}^i)$. Since that $p(\bar{X}^i)$ have no influence on classification, the category of \bar{X}^i can be further determined by:

$$h_{nb}(\bar{X}^i) = \arg \max_{c_k \in C} p(E^i | c_k) \cdot p(V_{up}^i | c_k) \cdot p(V_{down}^i | c_k) \cdot p(T_{ave}^i | c_k) \cdot p(T_{max}^i | c_k) \cdot p(c_k) \quad (7)$$

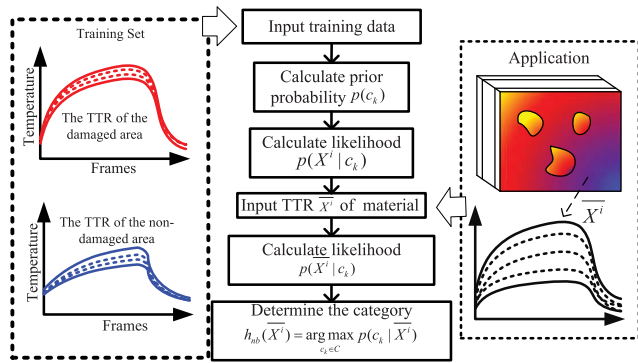


FIGURE 9. Bayesian framework.

where $p(\bar{X}^i|c_k)$ and $p(c_k)$ can be trained from historical data. $h_{nb}(\bar{X}^i)$ represents the final category of \bar{X}^i .

The developed algorithm replaces the previous classification methods by building the Bayesian classifier of transient temperature attributes. Since the Bayesian classifier is established by historical data as shown in Figure 9, the accuracy of the algorithm can be improved by applying the addition of prior information.

Remark 1: Since the damage assessment of HVI research is in its infancy, we don't have a large number of data. In addition, since that we need to detect the damage of spacecraft when it is in the orbit, the detection method should solve the problem quickly and efficiently. Some methods, such as, Random forest (RF), Deep learning, require a large number of samples to build up the classifier. Some methods, such as, Support Vector Machine (SVM), need a large number of iterations in the classification process, which makes some of these methods have low efficiency. Hence, these methods are not suitable for the damage assessment of HVI in the current. However, Bayesian classifier is a probabilistic method which can classify data quickly and efficiently. It has such steady theory basis and simple calculation. Hence, Bayesian classifier is firstly adopted to classify TTRs in the paper.

C. VISUALIZATION

To detect the damages of the hypervelocity impact damage and visualize the results, the detection process is shown in Table. 2:

In Step a), the global maximum temperature $S(I^*, J^*, T^*)$ is selected by the TCR $V(i, j) = \frac{S(i, j, t_{mid}) - S(i, j, t_0)}{t_{mid} - t_0}$. CL^u , RL^v are obtained to sample the image sequence. After that, the effective information of the thermal image matrix S is extracted by correlation comparison between sampling TTRs. In Step b), the classified information in different areas is mined by the developed Bayesian classifier established based on transient temperature attributes (E , V_{up} , V_{down} , T_{ave} , T_{max}). Step c) finds the regional center of each area $X_m^{c_k}$ by calculating the mean, and then selects the representative TTR $X_{re}^{c_k}$ of each category through the maximum-between-cluster-distance decision function. Step d) inverts damage image by solving linear model $L = \hat{G} * A^T$, and then

TABLE 2. The process of detection method.

Input: Thermal image sequence $S \in R^{N_I \times N_J \times N_T}$

Process:

- Variable-interval algorithm based on transient temperature attributes is used to obtain a represented TTRs set X , and the details are shown in Subsection III-B;
- Bayesian classifier is used to divide X into K categories, and the details are shown in Subsection III-B;
- The most effective represented TTR of each category is calculated as follows:

$$X_{re}^{c_k} = \arg \max_{\substack{x_i^{c_k}, i=1, \dots, N_{c_k} \\ k \neq \bar{k}}} \sum_{c_j \in \bar{k}} (\|X_i^{c_k} - X_m^{c_j}\|_2)$$
 where $X_m^{c_k}$ represents the center of each category. All representatives are used to form the matrix G ;
- Solve $L = \hat{G} * A^T$ to obtain images, where \hat{G} represents pseudo inverse, A is transformed from S . Then, the Canny operator is used to segment the image.

uses Canny operator to realize damage visualization. For the damage image, the image noise is removed by Gaussian filter

$h(l, h, \sigma) = \frac{\exp(-\frac{l^2+h^2}{2\sigma^2})}{2\pi\sigma}$. Then the gradient operators $G_x = g(l, h) - g(l + 1, h + 1)$, $G_y = g(l + 1, h) - g(l, h + 1)$ are used to obtain the gradient amplitude $G(l, h) = |G_l| + |G_h|$. Finally, the damage edge is extracted by comparing the high and low threshold H_{th} , L_{th} with the gradient amplitude $G(l, h)$, where g represents the de-noised image.

Remark 2: The detection of spacecraft materials plays an important role in the aerospace field. The method proposed in this paper uses the infrared image sequence to detect the damage of the material in a non-destructive way. The main steps of the proposed method are as follows: Firstly, a variable-interval method is proposed to extract effective information from image sequence. Hence, the efficiency of the method can be improved. The details are explained in Section III-A. Secondly, TTRs are described by establishing physical attributes (E , V_{up} , V_{down} , T_{ave} , T_{max}). After that, Bayesian classifier is used to judge TTRs in different damaged areas. The details are explained in Section III-B. Thirdly, the damage of the material is clearly shown with images. In addition, the Canny operator is applied to extract the texture of the damage, and this can lay the foundation for quantifying damage in the future.

IV. EXPERIMENTAL RESULTS

A. THE ESTABLISHMENT OF THE DETECTION FRAMEWORK

For the material with impact damage in Figure 12(a),

In this section, the detection framework is applied to detect materials of two types of damage (i.e. artificial damage, natural damage). It is worth mentioning that the test pieces in the figure are two different materials(that is, ceramic material and aluminum material). Since the difference in thermal conductivity between the two materials, different NB classifiers



FIGURE 10. Hypervelocity ballistic range.

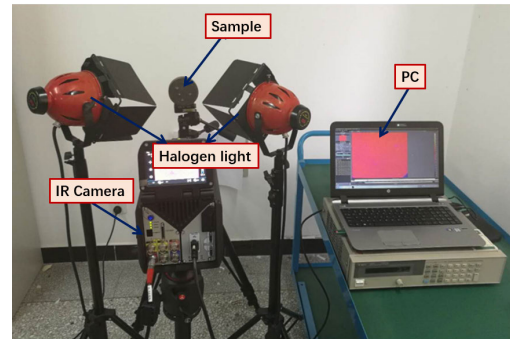


FIGURE 11. Experimental set-up.

TABLE 3. The performance comparison of the classifier.

| damage | F-score | Accuracy | AUC |
|------------|---------|----------|--------|
| Impact | 94.23% | 96.15% | 0.9495 |
| Artificial | 95.82% | 95.00% | 1.00 |

need to be built with the historical data of two materials respectively. For the material with impact damage, the Al-alloy projectiles in $\Phi 3$ mm are fired from a two-stage light-gas-gun (LGG) of China Aerodynamics Research and Development Center (CARDC) in Figure 10.

After these hypervelocity impact tests, the infrared camera is applied to record the surface heat distribution of the thermal protection materials excited thermally by halogen lights, as shown in Figure 11. The $T = 330$ frames in image sequences are collected. For the material with impact damage, 300 TTRs from historical data are used to train the NB. Five attributes ($E^i, V_{up}^i, V_{down}^i, T_{ave}^i, T_{max}^i$) are computed and then they are used to build a NB, which can divide TTRs of natural damage into damaged area and non-damaged area. Finally, 156 TTRs, which are different from the 300 train samples, are used to test the performance of NB for natural damage detection. For the material with artificial damage in Figure 12, the $T = 240$ frames in image sequences are collected. Moreover, 200 TTRs from historical data are used to train the NB. The establishment process is the same as that for natural damage. Then a NB is obtained and it can be used to divide TTRs of artificial damage into two different damaged areas and non-damaged area. Finally, 80 TTRs are used to test the performance of NB for artificial damage detection. The F-score, accuracy, AUC are used to evaluate the performance of the NB, the definition of these parameters are shown in the Appendix, the results are shown in Table 5. Through these parameters, both natural and artificial damage information can be mined by the NB classifiers.

B. THE APPLICATION OF THE DETECTION FRAMEWORK

Case 1: For the natural damage detection, the thresholds are given by $T(q)$ ($T(1) = 29.0351, T(2) = 29.2742$) and $T(p)$ ($T(1) = 29.1548, T(2) = 27.9390$), which divide the row and column into 3 blocks respectively. Next, the other thresholds are set as $Th_{RL}^1 = 0.99, Th_{RL}^2 = 0.90, Th_{RL}^3 = 0.99, Th_{CL}^1 = 0.99, Th_{CL}^2 = 0.93, Th_{CL}^3 = 0.98, Th = 0.78$.



FIGURE 12. The material with artificial damage.

After that, the intervals of step are obtained ($RL^1 = 9, RL^2 = 3, RL^3 = 5, CL^1 = 3, CL^2 = 3, CL^3 = 7$). Finally, set $Th = 0.78$, then 301 TTRs are selected from the infrared image sequence.

Then, NB established in Section IV-A is used to judge the areas of 301 TTRs. Firstly, the five attributes of each TTR are computed as follows: $E^i = \|X^i\|_2^2 = x_1^{i2} + \dots + x_{330}^{i2}$, $V_{up}^i = \frac{x_{100}^i - x_1^i}{100 - 1}, V_{down}^i = \frac{x_{250}^i - x_{300}^i}{300 - 250}, T_{ave}^i = \frac{x_1^i + \dots + x_{330}^i}{330}, T_{max}^i = \max_{t=1, \dots, 330} x_t^i$. After this step, NB for natural damage detection is used for classifying and the result is shown in Figure 13. 301 TTRs are divided into 2 categories, where 168 TTRs in the non-damaged position (the blue spots) and 133 TTRs in the damaged position (the red spots). After that, the representative TTR of each class is calculated (Section III-C, Step c)) and the results are as follows: $X_{re}^1 = X_1^2, X_{re}^2 = X_2^{71}$, where X_1^i, X_2^i represent the TTR of the non-damaged area and damaged area respectively. Then the representatives are used to analyze the advantages of the proposed method.

The representative TTRs of natural damage processed by proposed method, ICA [17], FCM [22] and the realistic situation are shown in Figure 14 to Figure 17 respectively, where blue curves and red curves represent TTRs in the non-damaged area and damaged area respectively. Since the damaged is doped with air, which has better thermal conductivity, the temperature of this area changes dramatically. By contrast, the temperature of non-damaged area changes relatively gentle. By comparison, since all the attributes are different, the feature space can be used for extracting the

TABLE 4. The attribute values of different methods.

| Area | Method | E | V_{up} | V_{down} | T_{ave} | T_{max} |
|------------------|---------|-----------|-------------|--------------|-----------|-----------|
| Damaged area | NB | $3.32e^5$ | $3.3e^{-2}$ | $7.6e^{-2}$ | 31.4 | 33.1 |
| | FCM | $3.70e^5$ | $3.9e^{-2}$ | $10.5e^{-2}$ | 33.1 | 35.3 |
| | ICA | 55.4 | $0.1e^{-2}$ | $0.6e^{-2}$ | 0.36 | 0.53 |
| | Reality | $2.96e^5$ | $1.6e^{-2}$ | $4.1e^{-2}$ | 29.7 | 31.1 |
| Non-damaged area | NB | $2.60e^5$ | $0.8e^{-2}$ | $1.6e^{-2}$ | 27.8 | 28.7 |
| | FCM | $2.63e^5$ | $0.6e^{-2}$ | $1.6e^{-2}$ | 28.0 | 28.8 |
| | ICA | 39.3 | $0.1e^{-2}$ | $0.3e^{-2}$ | 0.33 | 0.46 |
| | Reality | $2.43e^5$ | $0.3e^{-2}$ | $0.5e^{-2}$ | 26.9 | 27.3 |

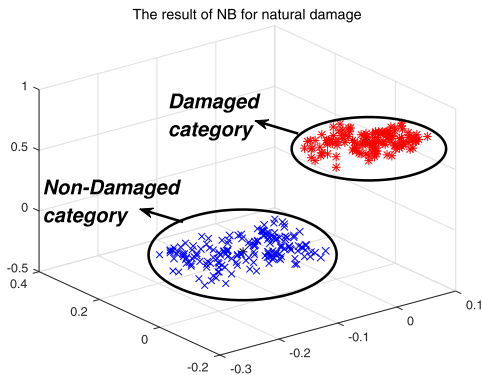


FIGURE 13. The result under Bayesian classifier.

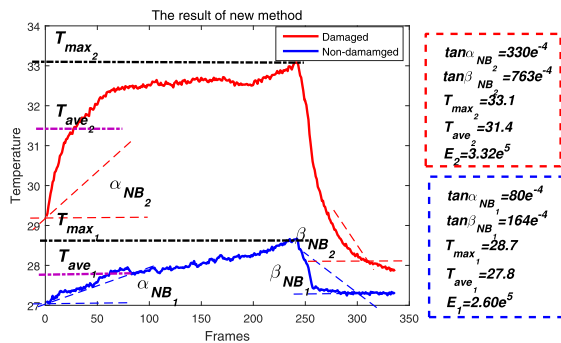


FIGURE 14. The result of the proposed method.

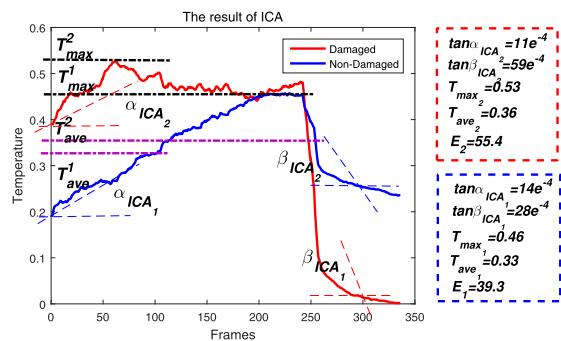


FIGURE 15. The result of ICA.

information in different areas. In addition, through the comparison of the specific attribute values shown in Table 4, the attribute values of the proposed method are similar to

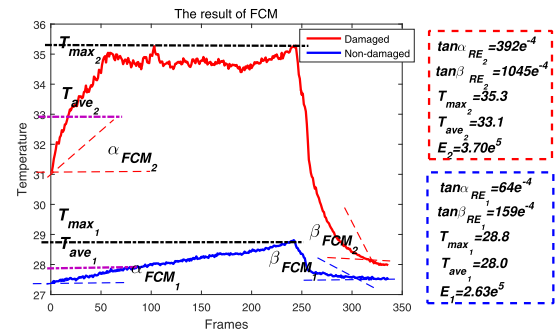


FIGURE 16. The result of FCM.

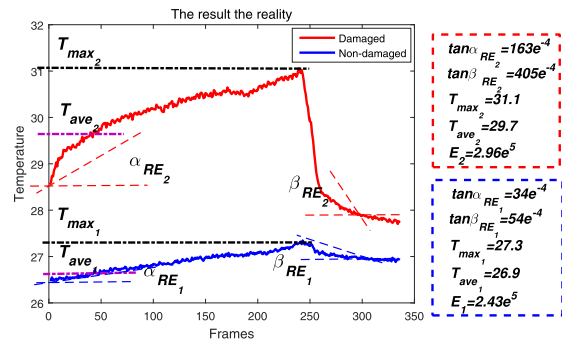
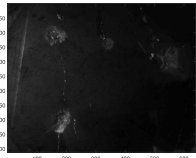
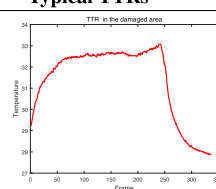
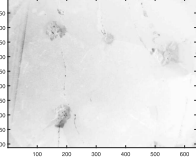
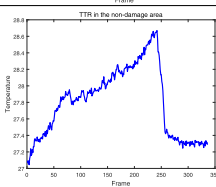


FIGURE 17. The reality.

that of the reality. That means the result of ICA does not have practical significance in the feature space. In addition, the results of new method is more accurate than that of FCM through the comparison of the results of these two methods. Comparing with the values of these attributes in Table 4, it can be found that the developed detection method based on the NB classifier has better performance of seeking TTRs, to evaluate effectively the HVI damage. In total, the proposed attributes are effective for the extraction of the natural damage information and the proposed method is more accurate than ICA and FCM.

Finally, in order to visualize the damage, solving the equation in Section III-C Step d) to obtain 2-dimensional images. The results are shown in Table 5, where the first column contains the images and the second presents the corresponding TTRs. After that, the Canny operator is used to process Figure 18, the high threshold and the low threshold are set as 0.4 and 0.2 respectively, and the result is shown in Figure 19.

TABLE 5. The results of method.

| NO. | RGB Figures | Typical TTRs |
|------|---|---|
| TTR1 |  |  |
| TTR2 |  |  |

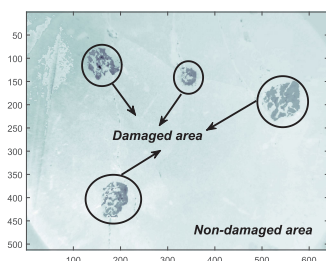


FIGURE 18. 2-D image information.

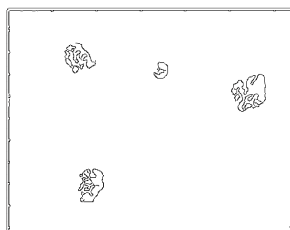


FIGURE 19. The outline of the damage areas.

Remark 3: Artificial-selection means that we manually select the TTRs of different types of damages in the standard material. These TTRs are considered as the criteria for evaluating different experimental results. The standard material is a material with known damage. In the process of manually selecting TTRs, we heat the standard material, and then find the Artificial-selection TTRs in the infrared image sequence corresponding to the damaged areas.

Case 2: For the artificial damage detection, set the temperature thresholds as $T(q)$ ($T(1) = 30.1114$, $T(2) = 30.4364$) and $T(p)$ ($T(1) = 33.0704$, $T(2) = 34.5647$). Then the thresholds are set as follows: $Th_{RL}^1 = 0.9986$, $Th_{RL}^2 = 0.9990$, $Th_{RL}^3 = 0.9950$, $Th_{CL}^1 = 0.9995$, $Th_{CL}^2 = 0.9995$, $Th_{CL}^3 = 0.9995$. After that, the interval of steps are expressed as follows: $RL^1 = 1$, $RL^2 = 7$, $RL^3 = 5$, $CL^1 = 5$, $CL^2 = 3$, $CL^3 = 3$. Finally, set $Th = 0.98$, then 383 TTRs are selected from the data block.

Then, the NB for artificial damage detection is used to identify the areas of 383 TTRs. Firstly, attributes are

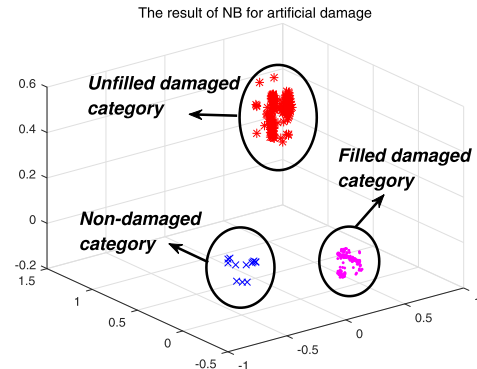


FIGURE 20. The result under the Bayesian classifier.

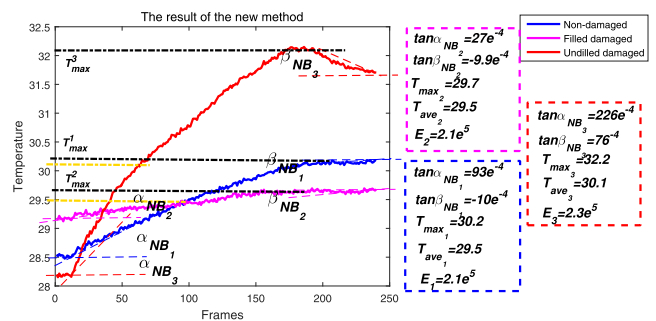


FIGURE 21. The result of the proposed method.

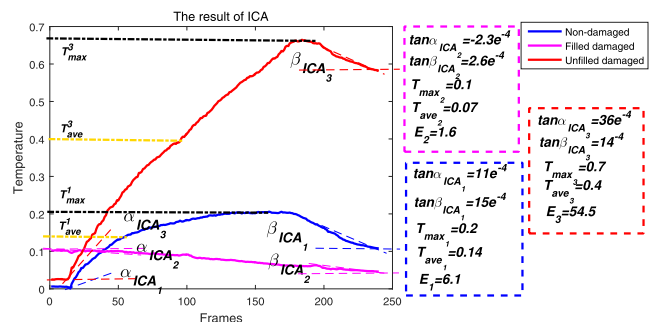


FIGURE 22. The result of ICA.

calculated as follows: $E^i = \|X^i\|_2^2 = x_1^2 + \dots + x_{240}^2$, $V_{up}^i = \frac{x_{185}^i - x_{11}^i}{185 - 11}$, $V_{down}^i = \frac{x_{185}^i - x_{240}^i}{240 - 185}$, $T_{ave}^i = \frac{x_1^i + \dots + x_{240}^i}{240}$, $T_{max}^i = \max_{t=1, \dots, 240} x_t^i$. After this step, they are put into NB. The result of the classification is shown in Figure 20, where 13 TTRs in the non-damaged position (the blue part), 187 TTRs in the stuffed-hole damaged area (the pink part) and 183 TTRs in the through-hole damaged area (the red part). After that, the representative TTR of each category is calculated and the results are as follows $X_{re}^1 = X_1^2$, $X_{re}^2 = X_2^{145}$, $X_{re}^3 = X_3^2$, where X_1^i , X_2^i and X_3^i represent the non-damaged category, stuffed-hole damaged category and through-hole damaged category respectively. Then, these TTRs are used to explain the performance of the proposed algorithm.

The representative TTRs of artificial damage processed by proposed method, ICA [17], FCM [22] and the realistic

TABLE 6. The attribute values of different methods.

| Area | Method | E | V_{up} | V_{down} | T_{ave} | T_{max} |
|------------------|---------|----------|---------------|---------------|-----------|-----------|
| Damage <i>i</i> | NB | $2.3e^5$ | $2.3e^{-2}$ | $0.8e^{-2}$ | 30.1 | 32.2 |
| | FCM | $2.2e^5$ | $1.8e^{-2}$ | $0.6e^{-2}$ | 30.1 | 31.2 |
| | ICA | 54.5 | $0.4e^{-2}$ | $0.1e^{-2}$ | 0.7 | 0.4 |
| | Reality | $2.3e^5$ | $2.5e^{-2}$ | $2.2e^{-2}$ | 31.0 | 32.4 |
| Damage <i>ii</i> | NB | $2.1e^5$ | $0.27e^{-2}$ | $-0.1e^{-2}$ | 29.5 | 29.7 |
| | FCM | $2.0e^5$ | $0.28e^{-2}$ | $-0.21e^{-2}$ | 29.2 | 29.5 |
| | ICA | 1.6 | $-0.02e^{-2}$ | $0.03e^{-2}$ | 0.07 | 0.1 |
| | Reality | $2.1e^5$ | $0.25e^{-2}$ | $-0.16e^{-2}$ | 29.5 | 29.7 |
| Non-damaged | NB | $2.1e^5$ | $0.93e^{-2}$ | $-0.1e^{-2}$ | 29.5 | 30.2 |
| | FCM | $2.1e^5$ | $1.2e^{-2}$ | $0.04e^{-2}$ | 29.6 | 30.5 |
| | ICA | 6.1 | $0.1e^{-2}$ | $0.15e^{-2}$ | 0.14 | 0.2 |
| | Reality | $2.1e^5$ | $1.3e^{-2}$ | $0.06e^{-2}$ | 29.7 | 30.6 |

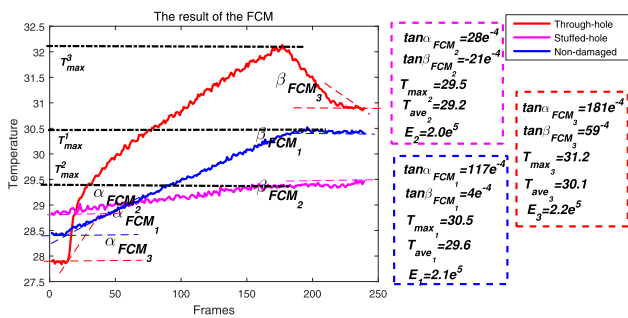


FIGURE 23. The result of FCM.

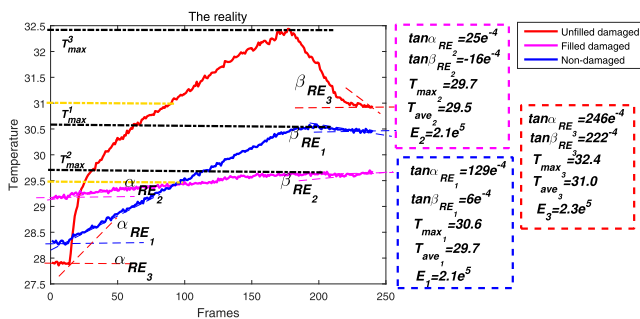


FIGURE 24. The reality.

situation are shown in Figures 21-24 respectively, where blue, red and pink curves represent TTRs in the non-damaged area, through-hole damaged area and stuffed-hole damaged area respectively. Since the through-hole damage is doped with more air, the temperature changes drastically in the damaged area. However, there is no air in non-damaged area. Thus the temperature change is relatively gentle in this area. By contrast, since the material in the stuffed-hole damage has a the poor thermal conductivity, the temperature changes in this area is the most gentle. All the attributes are unequal in different areas, that means the feature space is effective for information extraction. As shown in Table 6, the specific attribute values of the proposed method are similar to that of the reality. That means the proposed method takes into account the physical meaning of TTRs. In addition, by comparing the results of proposed method and that of FCM.

TABLE 7. The results of method.

| NO. | RGB Figures | Typical TTRs |
|------|-------------|--------------|
| TTR1 | | |
| TTR2 | | |
| TTR3 | | |

Although TTR of FCM is more closer to the reality in the non-damaged area, the results of the proposed method are more accurate in other two damaged areas. Hence, the proposed method is better than FCM. In summary, the proposed method can mine the artificial damage information based on attributes and the result is more accurate than ICA and FCM.

Finally, the Canny operator is used to extract the damaged areas. The first step is to reverse 2-dimensional images using the method in Section III-C Step d). The results are shown in Table 7. After that, the Canny operator is used to process Figure 25, the high threshold and the low threshold are set as 0.1 and 0.05 respectively, the edges of the damages are shown in Figure 26.

Remark 4: It should be emphasized that in the damage assessment of HVI, we need to describe the damage in detail. As shown in Figure 19 and Figure 26, we use Canny operator to extract the texture distribution of the damage, and we can clearly see the damage of different materials through the damage texture information. Furthermore, we plan to quantify the

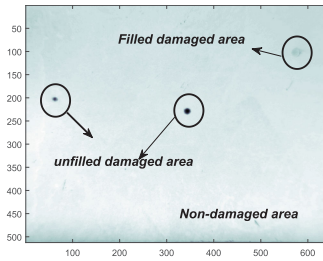


FIGURE 25. 2-D image information.

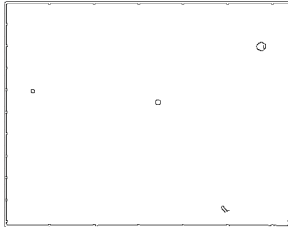


FIGURE 26. The outline of the damage areas.

damage, such as, area, circumference, etc., using this texture information in the future.

V. CONCLUSION

In this paper, a method for detecting HVI is proposed. In the experiment, the NB for materials of different types of damage are established by the historical data. For the natural damage detection, the accuracy, F-score and AUC of NB are 91.15%, 94.23% and 0.9495 respectively. For the artificial damage detection, the accuracy, F-score and AUC of NB are 95.00%, 95.82% and 1 respectively. Then, the proposed method is used for hypervelocity impact damage detection. By comparison with the result of the proposed method, ICA and FCM, we find that the accuracy of the proposed method is better than that of ICA and FCM. In addition, the proposed method is better combined with physical meaning. In total, the detection framework is an effective way in the field of infrared detection for hypervelocity impact.

In the future work, weakening the conditional independence assumption of NB and selecting the appropriate classifier for different data are the focus of the work. In addition, it is worth mentioning that changes in the external environment will have a non-negligible impact on data acquisition. Hence, we will also investigate how to investigate multiple environments in the detection framework in future.

APPENDIX

The F-score, accuracy, AUC [23], [33] are used to evaluate the performance, namely $F = \frac{2 \times \text{macro.P} \times \text{macro.R}}{\text{macro.P} + \text{macro.R}}$, $\text{Accuracy} = \frac{TP+TN}{TP+TN+FN+FP}$, $\text{TPR} = \frac{TP}{TP+FN}$, $\text{FPR} = \frac{FP}{TN+FP}$ where $\text{macro.P} = \sum_{i=1}^n P_i/n$, $\text{macro.R} = \sum_{i=1}^n R_i/n$, $P = TP/(TP+FP)$, $R = TP/(TP+FN)$. True positive (TP) represents TTRs belonging to damaged region correctly predicted as belonging to the damaged category. True negative (TN) represents typical TTRs correctly predicted as

belonging to the non-damaged category. False positive (FP) represents TTRs predicted as non-damaged category which real belong to damaged category. False negative (FN) represent typical TTRs predicted as damaged category which come from non-damaged category. FPR and TPR are the horizontal and vertical coordinates of the ROC respectively. AUC is the area value below the ROC curve.

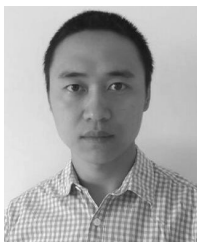
REFERENCES

- [1] Z. Yulin and W. Zhaokui, "Space traffic safety management and control," *IEEE Trans. Intell. Transp. Syst.*, vol. 17, no. 4, pp. 1189–1192, Apr. 2016.
- [2] B. Wei and B. D. Nener, "Multi-sensor space debris tracking for space situational awareness with labeled random finite sets," *IEEE Access*, vol. 7, pp. 36991–37003, 2019.
- [3] E. L. Christiansen, "Meteoroid/debris shielding," Lyndon B. Johnson Space Center, Nat. Aeronaut. Space Admin., Houston, TX, USA, Tech. Rep. TP-2003-210788, 2003.
- [4] J.-C. Liou and N. L. Johnson, "Risks in space from orbiting debris," *Science*, vol. 311, no. 5759, pp. 340–341, Jan. 2006.
- [5] E. L. Christiansen, J. Arnold, and B. Corsaro, "Handbook for designing MMOD protection," NASA Johnson Space Center, Houston, TX, USA, Tech. Rep. NASA/TM-2009-214785, 2009.
- [6] A. Falsone and M. Prandini, "A randomized approach to probabilistic footprint estimation of a space debris uncontrolled reentry," *IEEE Trans. Intell. Transp. Syst.*, vol. 18, no. 10, pp. 2657–2666, Oct. 2017.
- [7] X. Huang, C. Yin, J. Huang, X. Wen, Z. Zhao, J. Wu, and S. Liu, "Hypervelocity impact of TiB₂-based composites as front bumpers for space shield applications," *Mater. Des.*, vol. 97, pp. 473–482, May 2016.
- [8] X. Huang, C. Yin, H. Ru, S. Zhao, Y. Deng, Y. Guo, S. Liu, "Hypervelocity impact damage behavior of B4C/Al composite for MMOD shielding application," *Mater. Des.*, vol. 186, 2020, Art. no. 108323.
- [9] T. Maury, P. Loubet, M. Trisolini, A. Gallice, G. Sonnemann, and C. Colombo, "Assessing the impact of space debris on orbital resource in life cycle assessment: A proposed method and case study," *Sci. Total Environ.*, vol. 667, pp. 780–791, Jun. 2019.
- [10] Y. Fang and J. Pan, "Effects of space-based nanosecond pulse laser driving centimeter-sized space debris in LEO," *Optik*, vol. 180, pp. 96–103, Feb. 2019.
- [11] E. Watson, M. Gulde, L. Kortmann, M. Higashide, F. Schaefer, and S. Hiermaier, "Optical fragment tracking in hypervelocity impact experiments," *Acta Astronautica*, vol. 155, pp. 111–117, Feb. 2019.
- [12] M. Barus, H. Welemane, V. Nassiet, M. Pastor, A. Cantarel, F. Collombet, L. Crouzeix, and Y. Grunevald, "NDT-based design of joint material for the detection of bonding defects by infrared thermography," *NDT & E Int.*, vol. 93, pp. 157–163, Jan. 2018.
- [13] M. Ishikawa, H. Hatta, and S. Utsunomiya, "Effects of heating duration on pulse phase thermographic non-destructive testing," *Infr. Phys. Technol.*, vol. 61, pp. 216–223, Nov. 2013.
- [14] X. Maldague, *Theory and Practice of Infrared Technology for Nondestructive Testing*. New York, NY, USA: Wiley, 2001.
- [15] B. Gao, L. Bai, W. L. Woo, G. Y. Tian, and Y. Cheng, "Automatic defect identification of eddy current pulsed thermography using single channel blind source separation," *IEEE Trans. Instrum. Meas.*, vol. 63, no. 4, pp. 913–922, Apr. 2014.
- [16] A. A. Khan, V. Vrabie, J. I. Mars, A. Girard, and G. D'urso, "A source separation technique for processing of thermometric data from fiber-optic DTS measurements for water leakage identification in dikes," *IEEE Sensors J.*, vol. 8, no. 7, pp. 1118–1129, Jul. 2008.
- [17] T. Liang, W. Ren, G. Y. Tian, M. Elradi, and Y. Gao, "Low energy impact damage detection in CFRP using eddy current pulsed thermography," *Compos. Struct.*, vol. 143, pp. 352–361, May 2016.
- [18] L. Han, C. W. Li, S. L. Guo, and X. W. Su, "Feature extraction method of bearing AE signal based on improved FAST-ICA and wavelet packet energy," *Mech. Syst. Signal Process.*, vols. 62–63, pp. 91–99, Oct. 2015.
- [19] N. Rajic, "Principal component thermography for flaw contrast enhancement and flaw depth characterisation in composite structures," *Compos. Struct.*, vol. 58, no. 4, pp. 521–528, Dec. 2002.
- [20] P. Zhu, C. Yin, Y. Cheng, X. Huang, J. Cao, C.-M. Vong, and P. K. Wong, "An improved feature extraction algorithm for automatic defect identification based on eddy current pulsed thermography," *Mech. Syst. Signal Process.*, vol. 113, pp. 5–21, Dec. 2018.

- [21] X. Huang, C. Yin, and S. Dadras, "Adaptive rapid defect identification in ECPT based on K-means and automatic segmentation algorithm," *J. Ambient Intell. Humanized Comput.*, pp. 1–18, Jan. 2018, doi: [10.1007/s12652-017-0671-5](https://doi.org/10.1007/s12652-017-0671-5).
- [22] C. Yin, T. Xue, X. Huang, Y. H. Cheng, S. Dadras, and S. Dadras, "Research on damages evaluation method with multi-objective feature extraction optimization scheme for M/OD impact risk assessment," *IEEE Access*, vol. 7, pp. 98530–98545, 2019.
- [23] Ö. F. Arar and K. Ayan, "A feature dependent Naïve Bayes approach and its application to the software defect prediction problem," *Appl. Soft Comput.*, vol. 59, pp. 197–209, Oct. 2017.
- [24] Z. Duan, L. Wang, and M. Sun, "Model matching: A novel framework to use clustering strategy to solve the classification problem," *IEEE Access*, vol. 7, pp. 76227–76240, 2019.
- [25] P. R. N. Da Silva, H. A. Gabbar, P. Vieira, Jr., and C. T. Da Costa, Jr., "A new methodology for multiple incipient fault diagnosis in transmission lines using QTA and Naïve Bayes classifier," *Int. J. Elect. Power Energy Syst.*, vol. 103, pp. 326–346, Dec. 2018.
- [26] Z. Tang, L. Huang, X. Zhang, and H. Lao, "Robust image hashing based on color vector angle and Canny operator," *AEU-Int. J. Electron. Commun.*, vol. 70, no. 6, pp. 833–841, Jun. 2016.
- [27] X. Lyu, F. Liu, and P. Ren, "An Image processing approach to measuring the sphericity and roundness of fracturing proppants," *IEEE Access*, vol. 7, pp. 16078–16087, 2019.
- [28] S. Dong, D. Liu, R. Ouyang, Y. Zhu, L. Li, T. Li, and J. Liu, "Second-order Markov assumption based Bayes classifier for networked data with heterophily," *IEEE Access*, vol. 7, pp. 34153–34161, 2019.
- [29] S. Li, K. Zhang, J. Yin, and K. Yang, "A study on IR target recognition approach in aerial jamming environment based on Bayesian probabilistic model," *IEEE Access*, vol. 7, pp. 50300–50316, 2019.
- [30] B. Aviad and G. Roy, "Classification by clustering decision tree-like classifier based on adjusted clusters," *Expert Syst. Appl.*, vol. 38, no. 7, pp. 8220–8228, Jul. 2011.
- [31] Y. Li, E. Hung, and K. Chung, "Building a decision cluster classification model for high dimensional data by a variable weighting k-means method," in *Proc. Australas. Joint Conf. Artif. Intell.* Berlin, Germany: Springer, 2008, pp. 337–347.
- [32] R. Gelbard, O. Goldman, and I. Spiegler, "Investigating diversity of clustering methods: An empirical comparison," *Data Knowl. Eng.*, vol. 63, no. 1, pp. 155–166, Oct. 2007.
- [33] Siuly, H. Wang, and Y. Zhang, "Detection of motor imagery EEG signals employing Naïve Bayes based learning process," *Measurement*, vol. 86, pp. 148–158, May 2016.



HAONAN ZHANG received the B.Sc. degree in microelectronics science and engineering from the School of Electronic Engineering, Xian University of Posts and Telecommunications, Xi'an, China, in 2017. He is currently pursuing the M.Sc. degree in control engineering from the School of Automation Engineering, University of Electronic Science and Technology of China, Chengdu, China. His research interests include image processing, Bayesian inference, machine learning, and neural networks.



XUEGANG HUANG received the B.S. degree in materials science and engineering from Southwest Jiaotong University, and the M.S. and Ph.D. degrees from the Mechanical Engineering College, Shijiazhuang, China, in 2010 and 2014, respectively. His master's thesis was selected as the Excellent Master Dissertation of Hebei Province, in 2012 and his Ph.D. dissertation was selected as the National Excellent Doctoral Dissertation of China, in 2017.

He has been working as an Associate Researcher with the Hypervelocity Aerodynamic Institute, China Aerodynamics Research and Development Center, China, since 2014. He has published more than 60 refereed journal articles in the above-mentioned fields. His research interests are in spacecraft measurement and control technology, space shielding engineering, hypervelocity impact engineering and material dynamic behavior.



CHUN YIN (Member, IEEE) received the Ph.D. degree from the University of Electronic Science and Technology of China, in 2014. From 2011 to 2012, she was an Exchange Ph.D. Student with the Center for Self-Organizing and Intelligent Systems, Department of Electrical and Engineering, Utah State University, Logan, UT, USA. From 2012 to 2013, she was an Exchange Ph.D. Student with the MESA Lab, University of California, Merced, CA, USA. She was an Associate Professor with the University of Electronic Science and Technology of China, from 2014 to 2019. She has been a Professor with the School of Automation Engineering, University of Electronic Science and Technology of China, since 2019. Her research interests include multiobjective evolutionary optimization, infrared thermography testing, and hypervelocity impact engineering.

Seven of her articles have been listed as HOT article by Essential Science Indicators (ESI). One of her articles has been selected as the Top 5 list of Highly Cited Research in the journal of Mechatronics, and one of her articles has been selected as the ScienceDirect Top 25 list of Most Download Articles. She received the Overall Best Paper Award in 2015 IEEE International Instrumentation and Measurement Technology Conference. She received the Best New Scholars Award of University of Electronic Science and Technology of China. One of her technological achievements obtained the first prize for Scientific and Technological Progress Awards of Sichuan Province.



YU-HUA CHENG received the M.S. degree in measurement technology and industrial automation from Xihua University, in 2004, and the Ph.D. degree in measurement technology and industrial automation from Sichuan University, Chengdu, China, in 2007. He is currently working as a Professor with the University of Electronic Science and Technology of China. His research interests are in industrial automation and instrumentation, damage detection technique, and fault diagnosis.



ANHUA SHI received the B.Sc. degree in fluid mechanics from the Nanjing University of Aeronautics and Astronautics, Nanjing, China, in 2002. He is currently working as a Professor with the Hypervelocity Aerodynamic Institute, China Aerodynamics Research and Development Center. His research interests include infrared thermal imaging, radiation detection technology, and digital image recognition.



SARA DADRAS (Senior Member, IEEE) received the B.Sc. degree in electrical engineering from Shiraz University, in 2006, and the M.Sc. and Ph.D. degrees in electrical engineering from Tarbiat Modares University, in 2008 and 2012, respectively. She joined the Electrical and Computer Engineering Department, Utah State University, in 2012, as a Research Fellow. Her current research interests include hybrid electric vehicles, autonomous vehicles, renewable energy systems,

image processing, and optimal controls. She is an Organizer of the SAE Electronics Technical Committee.

Dr. Dadras is a member of ASME and SAE. She currently serves as an Associate Editor for the IEEE TRANSACTIONS ON AUTOMATION SCIENCE AND ENGINEERING, IEEE ACCESS, *Asian Journal of Control and Complexity*.



JINYANG LUO received the B.S. degree in physical electronics engineering from Southeast University, in 1997, and the M.S. degree in instrumentation engineering from Sichuan University, in 2008. He is currently working as a Senior Engineer with the Hypervelocity Aerodynamic Institute, China Aerodynamics Research and Development Center. His research interests include hypervelocity impact measurement, dynamic mechanics, and damage detection.

...